Nanowire waveguide made from extremely anisotropic metamaterials

Y. J. Huang, W. T. Lu,[*] and S. Sridhar

Department of Physics and Electronic Materials Research Institute, Northeastern University, Boston, Massachusetts 02115, USA

(Received 28 April 2008; published 26 June 2008)

Exact solutions are obtained for all the modes of wave propagation along an anisotropic cylindrical waveguide. Closed-form expressions for the energy flow on the waveguide are also derived. For extremely anisotropic waveguide where the transverse permittivity is negative ($\varepsilon_\perp < 0$) while the longitudinal permittivity is positive ($\varepsilon_\parallel > 0$), only transverse magnetic (TM) and hybrid modes will propagate on the waveguide. At any given frequency the waveguide supports an infinite number of eigenmodes. Among the TM modes, at most only one mode is forward wave. The rest of them are backward waves which can have very large effective index. At a critical radius, the waveguide supports degenerate forward- and backward-wave modes with zero group velocity. These waveguides can be used as phase shifters and filters, and as optical buffers to slow down and trap light.

I. INTRODUCTION

Since the realization of negative refraction [1] in microwaves [2], there is renewed and intense interest in electromagnetic metamaterials. Negative refraction has added a new arena to physics, leading to new concepts such as perfect lens [3,4], superlens [3,5,6], and focusing by plano-concave lens [7,8]. Negative refraction has subsequently been realized in microwaves [9–13], THz waves, and optical wavelengths [14–16], in metamaterials made of wire and split-ring resonators [17] or photonic crystals [18–20].

Metamaterials are artificially fabricated structures possessing certain desirable properties which are not available in natural materials. Metamaterials can have double negative index [21] or single negative index. Metamaterials can be periodic, such as photonic crystals [22]. They can also be nonperiodic, such as the materials for cloaking [23]. They can also be made to be anisotropic and have indefinite index [24–26]. Indefinite index metamaterials can be used to make hyperlens [27,28]. This range of properties opens infinite possibilities to use matematerials in frequencies from microwave all the way up to the visible.

Wave propagation in waveguide of nanometer size [29] has unique properties. In this paper, we consider wave propagation along anisotropic nanowires. In the case where the transverse permittivity is negative while the longitudinal one is positive ($\varepsilon_\perp < 0, \varepsilon_\parallel > 0$), these indefinite index waveguides can support both forward and backward waves. High effective index can be obtained for these modes. These waveguides can also support degenerate modes which can be used to slow down and trap light.

In Sec. II, we derive the formulas for all the modes on the anisotropic cylinders. Exact solutions for all the modes and closed-form expressions for the energy flow will be obtained. Possible zero net-energy flow modes will also be discussed. The situation for trapping light is presented in Sec. III. In Sec. IV, we propose the realization of nanowires made of indefinite index medium, which is confirmed in finite-difference time-domain simulations. We conclude in Sec. V with possible applications for these anisotropic nanowires.

II. WAVE PROPAGATION AND ENERGY FLOW ON ANISOTROPIC CYLINDRICAL WAVEGUIDES

We consider wave propagation on a cylindrical waveguide. The axis of the waveguide is along the z direction as shown in Fig. 1. The waveguide is nonmagnetic and has an anisotropic optical property

$$\varepsilon_x = \varepsilon_y = \varepsilon_t \neq \varepsilon_z. \tag{1}$$

The waves will propagate along the cylinder axis with

$$\mathbf{E} = \mathbf{E}_0 e^{i(\beta z - \omega t)}, \quad \mathbf{H} = \mathbf{H}_0 e^{i(\beta z - \omega t)}. \tag{2}$$

Here β is the propagation wave number along the waveguide.

Due to the symmetry of the waveguide, all of the field components can be expressed in terms of the longitudinal components E_z and H_z. In the polar coordinate system, one has for the fields inside the waveguide $r < a$ with a the radius,

$$E_r = i \frac{1}{\varepsilon_t k_0^2 - \beta^2} \left(\beta \partial_r E_z + k_0 \frac{1}{r} \partial_\phi H_z \right),$$
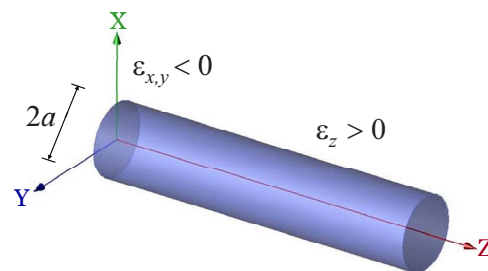
FIG. 1. (Color online) An anisotropic cylindrical waveguide with axis along the z axis. The longitudinal permittivity is positive while the transverse permittivity is negative.

*w.lu@neu.edu

$$E_\phi = i\frac{1}{\varepsilon_t k_0^2 - \beta^2}\left(\beta\frac{1}{r}\partial_\phi E_z - k_0\partial_r H_z\right),$$

$$H_r = i\frac{1}{\varepsilon_t k_0^2 - \beta^2}\left(-\varepsilon_t k_0\frac{1}{r}\partial_\phi E_z + \beta\partial_r H_z\right),$$

$$H_\phi = i\frac{1}{\varepsilon_t k_0^2 - \beta^2}\left(\varepsilon_t k_0\partial_r E_z + \beta\frac{1}{r}\partial_\phi H_z\right). \tag{3}$$

Here k_0 is the wave number in the vacuum.

The wave equations for the longitudinal components inside the waveguide are

$$(\partial_x^2 + \partial_y^2)E_z + \varepsilon_z(k_0^2 - \beta^2/\varepsilon_t)E_z = 0,$$

$$(\partial_x^2 + \partial_y^2)H_z + (\varepsilon_t k_0^2 - \beta^2)H_z = 0. \tag{4}$$

The waveguide is free standing in air, so the wave equations for $r > a$ are given by the above equations with the permittivity replaced by unity. The solutions are expressed in terms of the Bessel functions of various kinds

$$E_z = AJ_n(Kr)e^{in\phi}, \quad r < a,$$

$$= CK_n(\kappa_0 r)e^{in\phi}, \quad r > a \tag{5}$$

and

$$H_z = BI_n(\kappa r)e^{in\phi}, \quad r < a,$$

$$= DK_n(\kappa_0 r)e^{in\phi}, \quad r > a. \tag{6}$$

The coefficients will be determined by matching the boundary conditions. Here

$$K = \sqrt{\varepsilon_z}\sqrt{k_0^2 - \beta^2/\varepsilon_t},$$

$$\kappa = \sqrt{\beta^2 - \varepsilon_t k_0^2},$$

$$\kappa_0 = \sqrt{\beta^2 - k_0^2}. \tag{7}$$

We only consider the extremely anisotropic case such that the longitudinal permittivity is positive while the transverse permittivity is negative,

$$\varepsilon_z > 0, \quad \varepsilon_t < 0. \tag{8}$$

One can see that due to the anisotropic nature of the waveguide, H_z and E_z inside the waveguide will have completely different behaviors.

The continuity of E_z and H_z at the interface $r=a$ gives

$$\frac{C}{A} = \frac{J_n(Ka)}{K_n(\kappa_0 a)}, \quad \frac{D}{B} = \frac{I_n(\kappa a)}{K_n(\kappa_0 a)}. \tag{9}$$

The continuity of E_ϕ at the interface gives

$$in\beta\frac{\kappa_0^2 - \kappa^2}{k_0 a^2 \kappa_0^2 \kappa^2} = \frac{B}{A}\frac{I_n(\kappa a)}{J_n(Ka)}[g_n(\kappa_0 a) + h_n(\kappa a)] \tag{10}$$

with the following defined functions

$$g_n(x) = -\frac{K_n'(x)}{xK_n(x)} = \frac{K_{n-1}(x)}{xK_n(x)} + \frac{n}{x^2},$$

$$h_n(x) = \frac{I_n'(x)}{xI_n(x)} = \frac{I_{n-1}(x)}{xI_n(x)} - \frac{n}{x^2}. \tag{11}$$

The continuity of H_ϕ at the interface gives

$$in\beta\frac{\kappa^2 - \kappa_0^2}{k_0 a^2 \kappa_0^2 \kappa^2} = \frac{A}{B}\frac{J_n(Ka)}{I_n(\kappa a)}[g_n(\kappa_0 a) - \varepsilon_z f_n(Ka)] \tag{12}$$

with

$$f_n(x) = \frac{J_n'(x)}{xJ_n(x)} = \frac{J_{n-1}(x)}{xJ_n(x)} - \frac{n}{x^2}. \tag{13}$$

Thus we obtain the equation for all of the modes

$$[g_n(\kappa_0 a) - \varepsilon_z f_n(Ka)][g_n(\kappa_0 a) + h_n(\kappa a)]$$

$$= n^2[(\kappa_0 a)^{-2} - (\kappa a)^{-2}][(\kappa_0 a)^{-2} - \varepsilon_t(\kappa a)^{-2}]. \tag{14}$$

For wave propagation on the cylindrical waveguide, the components of the Poynting vector are

$$S_z = \frac{1}{4\pi}(E_r H_\phi^* - E_\phi H_r^*),$$

$$S_r = -\frac{1}{4\pi}(E_z H_\phi^* - E_\phi H_z^*),$$

$$S_\phi = \frac{1}{4\pi}(E_z H_r^* - E_r H_z^*). \tag{15}$$

The physical Poynting vector is given by Re $\mathbf{S}$.

The total energy flow along the waveguide is the sum of energy flow inside and outside the waveguide

$$P_z = P_z^{in} + P_z^{out} \tag{16}$$

with

$$P_z^{in} = 2\pi\int_0^a S_z r\,dr, \quad P_z^{out} = 2\pi\int_a^\infty S_z r\,dr. \tag{17}$$

Following Ref. [30], the total energy flow is normalized as

$$\langle P_z \rangle = \frac{P_z^{in} + P_z^{out}}{|P_z^{in}| + |P_z^{out}|}. \tag{18}$$

Thus one has $-1 < \langle P_z \rangle < 1$.

In the following, we discuss different modes in detail.

A. TE modes

For the transverse electric (TE) modes, $E_z=0$. The longitudinal magnetic field is given by Eq. (6). One has

$$E_\phi = i\frac{k_0}{\kappa^2}\partial_r H_z = i\frac{k_0}{\kappa}BI_1(\kappa r), \quad r < a,$$

$$= i\frac{k_0}{\kappa_0^2}\partial_r H_z = -i\frac{k_0}{\kappa_0}DK_1(\kappa r), \quad r > a. \tag{19}$$

The continuity of E_ϕ at the interface requires that

$$h_0(\kappa a) + g_0(\kappa_0 a) = 0. \tag{20}$$

For materials without loss, each term on the left-hand side is positive, thus there is no solution. The waveguide does not support TE modes. This is exactly like that of a metallic wire which does not support TE surface waves since current must flow along the waveguide.

Only when $\varepsilon_t > 1$, the waveguide will support TE modes, like an ordinary dielectric fiber.

B. TM modes

For the transverse magnetic (TM) modes, $H_z = 0$. The longitudinal electric field is given by Eq. (5). One has

$$H_\phi = -i\varepsilon_z \frac{k_0}{K} A J_1(Kr), \quad r < a,$$

$$= i\frac{k_0}{\kappa_0} C K_1(\kappa_0 r), \quad r > a. \tag{21}$$

The continuity of H_ϕ leads to the equation

$$\varepsilon_z f_0(Ka) = g_0(\kappa_0 a). \tag{22}$$

The solutions to this equation give all the TM modes.

1. Band structure of TM modes

We first consider the solutions for fixed and real values of ε_z and ε_t. This is normally associated with a fixed k_0. It is convenient to consider solution in the form of Ka or the reduced radius $k_0 a$ as a function of $\kappa_0 a$. The wave number along the waveguide can be obtained through $\beta = (k_0^2 + \kappa_0^2)^{1/2}$. Before we seek general solutions, it is better to consider the solutions in certain limits to reveal some important features of the TM modes on the anisotropic waveguide.

For the TM modes close to the light line, $\kappa_0 a \to 0$, one has

$$Ka \simeq x_{0,m} - \frac{\varepsilon_z}{x_{0,m}}(\kappa_0 a)^2 \left(\ln \frac{\kappa_0 a}{2} + \gamma \right).$$

Here we have used $K_0(x) = -\ln(x/2) - \gamma$ for small argument with γ the Euler constant. For complex ε_t with Re $\varepsilon_t < 0$ and Im $\varepsilon_t > 0$, the real and imaginary parts of β of the allowed modes will have the same signs. These modes are forward waves, similar to that of an ordinary optical fiber. We note that close to the light line, the property of the TM modes of the anisotropic waveguide is similar to that of an isotropic fiber with $\varepsilon = 1 + \varepsilon_z(1 - \varepsilon_t^{-1})$.

In the limit of long wavelength or small waveguide radius, $k_0 a \ll 1$, Eq. (22) is reduced to

$$\varepsilon_z f_0(\kappa_0 a/\eta) = g_0(\kappa_0 a) \tag{23}$$

with $\eta = \sqrt{-\varepsilon_t/\varepsilon_z}$. This equation gives an infinite number of solutions $\kappa_0 a = \xi_{0,m}$ with $m = 1, 2, 3, \ldots$. This indicates that the anisotropic waveguide supports infinite number of propagating modes, no matter how thin the waveguide is. For $\kappa_0 a \to \infty$, since $g_0(\kappa_0 a) \simeq (\kappa_0 a)^{-1} \to 0$, one has $\xi_{0,m} \simeq \eta x_{1,m}$. Here $x_{n,m}$ is the mth zero of $J_n(x)$ away from the origin. For the mth TM band, one has $0 \le \kappa_0 a \le \xi_{0,m}$. The mth band starts
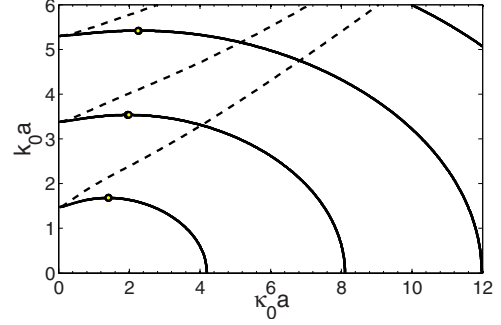

FIG. 2. (Color online) Band structure of the guided TM modes on an anisotropic waveguide of radius a with $\varepsilon_t = -3$ and $\varepsilon_z = 2$. Open circles denote the degenerate points of forward-wave and backward-wave modes. The dashed lines are for a dielectric waveguide with $\varepsilon = 1 + \varepsilon_z(1 - \varepsilon_t^{-1})$.

with $k_0 a = x_{0,m}/\sqrt{\varepsilon_z - \varepsilon_z/\varepsilon_t}$ when $\kappa_0 a = 0$ and ends at $k_0 a = 0$ when $\kappa_0 a = \xi_{0,m}$. The modes with $\kappa_0 \gg k_0$ have $d(k_0 a)/d(\kappa_0 a) < 0$ and are backward waves. It will be obvious if we include a small imaginary part in ε_t with Im $\varepsilon_t > 0$. The equation will give β with the real and imaginary parts having opposite signs. The energy flow is opposite to the phase velocity, which will be discussed later.

For arbitrary values of $\kappa_0 a$, the solution must be sought numerically. Since the right-hand side of Eq. (22) is always positive, the solution requires that $J_1(Ka)$ and $J_0(Ka)$ have different signs. For the mth band, since $0 \le \kappa_0 a \le \xi_{0,m}$ with $\xi_{0,m}$ the solutions of Eq. (23), one has $x_{0,m} \le Ka \le \xi_{0,m}/\eta < x_{1,m}$. For each $\kappa_0 a$ value, the Ka value can be searched within $[x_{0,m}, x_{1,m}]$ to satisfy Eq. (22). Once the corresponding Ka is found, the reduced radius can be obtained as

$$k_0 a = \frac{\sqrt{(-\varepsilon_t/\varepsilon_z)(Ka)^2 - (\kappa_0 a)^2}}{\sqrt{1 - \varepsilon_t}}.$$

For the mth band, the corresponding transverse electric field E_z will have m nodes. The band structure for a waveguide with $\varepsilon_t = -3$ and $\varepsilon_z = 2$ is shown in Fig. 2. The effective index of the waveguide $n_{\text{eff}} \equiv \beta/k_0$ is also evaluated and plotted in Fig. 3.
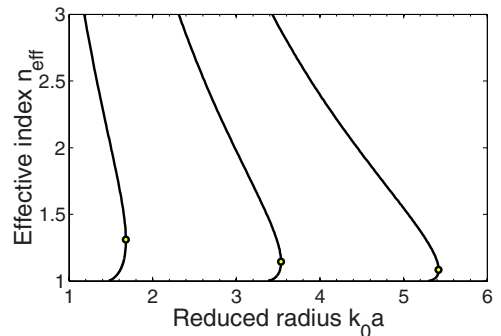

FIG. 3. (Color online) Effective index n_{eff} as a function of the reduced radius $k_0 a$ for the first three bands of TM modes on an anisotropic waveguide with $\varepsilon_t = -3$ and $\varepsilon_z = 2$. Open circles denote the degenerate points of forward-wave and backward-wave modes.
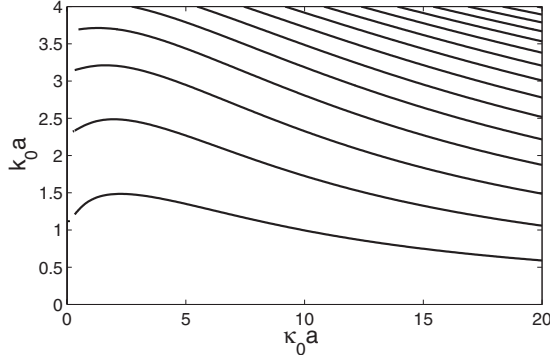
FIG. 4. Band structure of the guided TM modes on an anisotropic waveguide of radius a with ε_t and ε_z given by Eq. (24) with $a=10/k_p$ and $\varepsilon_a=2.25$.

Unlike an ordinary fiber where for each band, $d(k_0a)/d(\kappa_0a)>0$, each TM band of the anisotropic waveguide starts with $d(k_0a)/d(\kappa_0a)>0$ for small κ_0a or near the light line. At certain value of κ_0a or k_0a which is marked in Fig. 2, $d(k_0a)/d(\kappa_0a)=0$. Further increasing κ_0a results in $d(k_0a)/d(\kappa_0a)<0$. The band ends at a finite $\kappa_0a=\xi_{0,m}$. Immediately below the point k_0a where $d(k_0a)/d(\kappa_0a)=0$, each band has two modes with opposite signs of $d(k_0a)/d(\kappa_0a)$. One mode is forward wave and the other backward wave. This will be discussed later in the paper.

We next consider a waveguide of a fixed radius a with the following permittivity:

$$\varepsilon_t = \frac{1}{2}(1 + \varepsilon_a - k_p^2/k_0^2),$$

$$\varepsilon_z = 2\varepsilon_a(k_0^2 - k_p^2)/[k_0^2(1 + \varepsilon_a) - k_p^2]. \quad (24)$$

Here ε_a and k_p are positive constants. The realization of this property will be discussed later in Sec. IV. If $k_0 < k_p/(1 + \varepsilon_a)^{1/2}$, one has $\varepsilon_t < 0$ and $\varepsilon_z > 0$. The band structure of the TM modes on this waveguide is obtained by numeric means and plotted in Fig. 4 with the corresponding effective index in Fig. 5. For this waveguide, there is no cutoff of κ_0a for each band. This is because as $k_0 \to 0$, $\varepsilon_z \simeq 2\varepsilon_a$ and $\varepsilon_t \to -\infty$, thus $\eta = \sqrt{-\varepsilon_t/\varepsilon_z} \to \infty$. The cutoff $\xi_{0,m} \simeq \eta x_{1,m} \to \infty$.
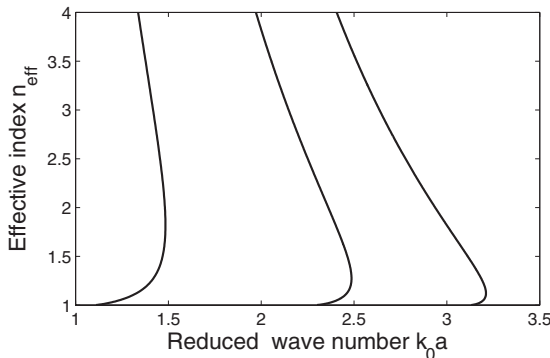

FIG. 5. Effective index n_{eff} as a function of the reduced wave number k_0a for the first three bands of TM modes on an anisotropic waveguide with ε_t and ε_z given by Eq. (24) with $a=10/k_p$ and $\varepsilon_a=2.25$.

We point out that the Padé approximant for the function $f_0(x) \equiv -x^{-1}J_1(x)/J_0(x)$ can be used to obtain a good estimate of the solutions. This will be discussed in the Appendix.

If $\varepsilon_t > 0$ and $\varepsilon_z < 0$, the waveguide also supports TM modes. The details will not be presented here.

2. Energy flow of TM modes

Within the waveguide, one has $E_z = AJ_0(Kr)$, $E_r = i(\varepsilon_z\beta/\varepsilon_tK)AJ_1(Kr)$, and $H_\phi = i(\varepsilon_zk_0/K)AJ_1(Kr)$. So the Poynting vector component along the axis of the waveguide is

$$S_z = \frac{\beta}{\varepsilon_tk_0a^2}\left|\frac{J_1(Kr)}{J_1(Ka)}\right|^2. \quad (25)$$

Here we set the coefficient $A = K/[\varepsilon_zk_0aJ_1(Ka)]$. Since $\varepsilon_t < 0$, the energy flow inside the nanowire is always opposite to the phase velocity.

For the field in the air $r > a$, one has $E_z = CK_0(\kappa_0r)$, $E_r = i(\beta\kappa_0)CK_1(\kappa_0r)$, and $H_\phi = i(k_0/\kappa_0)CK_1(\kappa_0r)$, thus

$$S_z = \frac{\beta}{k_0a^2}\left|\frac{K_1(\kappa_0r)}{K_1(\kappa_0a)}\right|^2. \quad (26)$$

Here the coefficient $C = -\kappa_0/[k_0aK_1(\kappa_0a)]$.

For the TM modes, one has

$$P_z^{in} = \frac{\beta}{2\varepsilon_tk_0a^2}\int_0^a\left|\frac{J_1(Kr)}{J_1(Ka)}\right|^2 rdr,$$

$$P_z^{out} = \frac{\beta}{2k_0a^2}\int_a^\infty\left|\frac{K_1(\kappa_0r)}{K_1(\kappa_0a)}\right|^2 rdr. \quad (27)$$

The above integrals can be carried out and more compact expressions for the energy flow can be obtained as

$$P_z^{in} = \frac{\beta}{4\varepsilon_tk_0(Ka)^2}\left(\frac{1}{f_0^2(Ka)} + \frac{2}{f_0(Ka)} + (Ka)^2\right)$$

$$= -\frac{\beta}{4k_0\varepsilon_z^2f_0^2(Ka)}\frac{\varepsilon_z^2f_0'(Ka)}{\varepsilon_tKa},$$

$$P_z^{out} = \frac{\beta}{4k_0(\kappa_0a)^2}\left(\frac{1}{g_0^2(\kappa_0a)} + \frac{2}{g_0(\kappa_0a)} - (\kappa_0a)^2\right)$$

$$= -\frac{\beta}{4k_0g_0^2(\kappa_0a)}\frac{g_0'(\kappa_0a)}{\kappa_0a}. \quad (28)$$

Here $g_0'(x)$ and $f_0'(x)$ are the derivatives of $g_0(x)$ and $f_0(x)$, respectively.

For convenience, we set $\beta > 0$ throughout the paper. Since $g_0'(x) < 0$ and $f_0'(x) < 0$, one has $P_z^{in} < 0$ and $P_z^{out} > 0$. In this convention, if $\langle P_z \rangle > 0$, this indicates that the energy flow and the phase propagation are in the same directions and the mode is a forward-wave mode. Otherwise $\langle P_z \rangle < 0$, the group velocity and the phase velocity are in the opposite direction and the mode is a backward-wave mode. The normalized energy flow for TM modes on a waveguide with $\varepsilon_t = -3$ and $\varepsilon_z = 2$ is shown in Fig. 6. We note that for some portion of the bands the value of $\langle P_z \rangle$ is negative and thus these modes are backward waves.
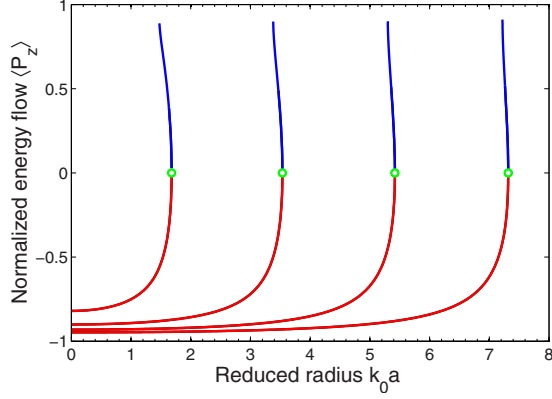
FIG. 6. (Color online) Normalized energy flow $\langle P_z \rangle$ for the first four bands of the TM modes on an anisotropic waveguide with $\varepsilon_t = -3$ and $\varepsilon_z = 2$. Here we set $\beta > 0$. Open circles denote the degenerate points where $\langle P_z \rangle = 0$.

3. Forward-wave and backward-wave TM modes

There are three ways to determine whether a mode is a forward wave or a backward wave. One is through the sign of the derivative $d(k_0 a)/d(\kappa_0 a)$. From the band structure, we have already noticed that for the modes near the light line, $d(k_0 a)/d(\kappa_0 a) > 0$. These modes are forward waves. For large $\kappa_0 a$ or small $k_0 a$, one has $d(k_0 a)/d(\kappa_0 a) < 0$, these modes are backward waves. From the band structure shown in Fig. 2, the majority of the modes are backward waves.

The second way is through the sign of $\langle P_z \rangle$. For the TM modes when $\kappa_0 a \to \infty$, one has $f_0(Ka) \to 0$ since $g_0(\kappa_0 a) \to 0$. One thus has $Ka \to x_{0,m}$. This solution leads to the divergence of P_z^{in} which is negative and the vanishing of P_z^{out} which is positive, subsequently $\langle P_z \rangle \to -1$, these modes are all backward waves. Correspondingly, one has $d(k_0 a)/d(\kappa_0 a) \to -\infty$ for $\kappa_0 a \to \infty$. This is evident from the band structure shown in Fig. 2.

In the following, we prove that $d(k_0 a)/d(\kappa_0 a) \geq 0$ leads to $\langle P_z \rangle \geq 0$ and vice versa. We consider the derivative

$$\frac{d(Ka)}{d(\kappa_0 a)} = -\frac{\varepsilon_z}{\varepsilon_t Ka}\left(\kappa_0 a + (1 - \varepsilon_t)k_0 a \frac{d(k_0 a)}{d(\kappa_0 a)}\right).$$

Thus one has

$$\frac{d(Ka)}{d(\kappa_0 a)} + \frac{\varepsilon_z \kappa_0 a}{\varepsilon_t Ka} \geq 0 \quad \text{if} \quad \frac{d(k_0 a)}{d(\kappa_0 a)} \geq 0.$$

On the other hand, according to the eigenequation $\varepsilon_z f_0(Ka) = g_0(\kappa_0 a)$, one has

$$\frac{d(Ka)}{d(\kappa_0 a)} = \frac{g_0'(\kappa_0 a)}{\varepsilon_z f_0'(Ka)}.$$

Making use of the above expression, one arrives at the inequality

$$-\frac{\varepsilon_z^2 f_0'(Ka)}{\varepsilon_t Ka} - \frac{g_0'(\kappa_0 a)}{\kappa_0 a} \geq 0,$$
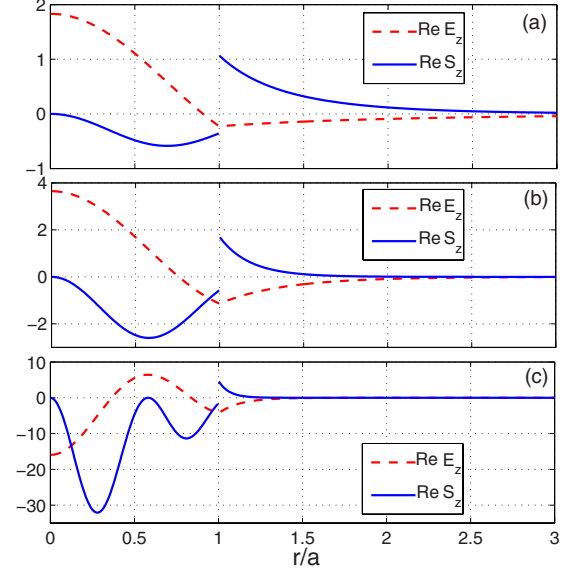
and subsequently

FIG. 7. (Color online) The longitudinal electric field and Poynting vector for the first three TM mode on an anisotropic waveguide of radius a with $\varepsilon_t = -3 + 0.05i$ and $\varepsilon_z = 2$ at $k_0 a = 1.6$ with (a) $\beta a = 1.7112 + 0.0067i$, (b) $\beta a = 2.7250 - 0.0397i$, (c) $\beta a = 7.5756 - 0.0676i$. The imaginary parts Im E_z and Im S_z are small and are not plotted.

$$P_z^{\text{in}} + P_z^{\text{out}} \geq 0 \quad \text{if} \quad \frac{d(k_0 a)}{d(\kappa_0 a)} \geq 0. \tag{29}$$

Similarly one has

$$P_z^{\text{in}} + P_z^{\text{out}} \leq 0 \quad \text{if} \quad \frac{d(k_0 a)}{d(\kappa_0 a)} \leq 0. \tag{30}$$

So the condition for $P_z = 0$ can be allocated from the band structures as shown in Figs. 2 and 4 when $d(k_0 a)/d(\kappa_0 a) = 0$.

The third way to determine whether a mode is a forward or backward wave is through the relative sign of the real and imaginary parts of β if dissipation is included. For example, we consider $\varepsilon_t = -3 + 0.05i$ and $\varepsilon_z = 2$. At $k_0 a = 1.6$, the wave numbers of the first three eigenmodes are $\beta a = \pm (1.7112 + 0.0067i)$, $\pm (2.7250 - 0.0397i)$, $\pm (7.5756 - 0.0676i)$. Since the free space wavelength is $\lambda = 3.927a$, this is a subwavelength waveguide. For the TM modes, except for the first mode, all the other modes are backward-wave modes since for those modes Re β and Im β have different signs. The normalized energy flow is $\langle P_z \rangle = 0.5151 - 0.0020i, -0.4002 - 0.0058i, -0.8760 - 0.0078$ for the above three modes, respectively. Here we set Re $\beta > 0$. The field and Poynting vector profiles are plotted in Fig. 7.

There is an interesting feature of the modes on the anisotropic waveguide. At a fixed k_0, for $a < a_m \equiv \sqrt{-\varepsilon_t/\varepsilon_z(1 - \varepsilon_t)} x_{0,m}/k_0$, the mth band TM modes are backward waves. If the radius $a > a_m$, the waveguide supports two TM modes for the mth band, one forward and one backward. At $a = a_c$, these two modes become degenerate and the total energy flow is zero. This can be seen in Figs. 2, 3, and 6 where degenerate points are marked. Further increasing the

radius, the waveguide will no longer support the mth band. The critical radius a_c is located such that $\langle P_z \rangle = 0$, $d(k_0 a)/d(\kappa_0 a) = 0$ or $dn_{\text{eff}}/da = \infty$. These degenerate modes can be used to slow down and even trap light. This will be discussed in the next section.

C. Hybrid modes

The modes with both $E_z \neq 0$ and $H_z \neq 0$ are called hybrid modes. Their dispersions are contained in the solutions of Eq. (14) with $n \neq 0$. We recast the equation in the following form:

$$\varepsilon_z f_n(Ka) = g_n(\xi) - \frac{n^2(\xi^{-2} - y^{-2})(\xi^{-2} - \varepsilon_t y^{-2})}{g_n(\xi) + h_n(y)}. \quad (31)$$

Here we use the notation $\xi = \kappa_0 a$ and $y = \kappa a$. Note that $Ka = y/\eta$ with $\eta = \sqrt{-\varepsilon_t/\varepsilon_z}$.

1. Band structure of hybrid modes

At a fixed wavelength λ or wave number k_0, ε_t, ε_z are constant. Since $Ka = y/\eta$, if we use $\xi = \kappa_0 a$ as a free parameter, the eigenequation gives a single value of Ka or y for each ξ. Since $y = \sqrt{\xi^2 + (1 - \varepsilon_t)(k_0 a)^2}$, so the eigenequation actually gives the reduced radius $k_0 a$ for each $\xi = \kappa_0 a$.

In the limit of long wavelength or small waveguide radius, $k_0 a \to 0$, Eq. (31) is reduced to

$$\varepsilon_z f_n(\xi/\eta) = g_n(\xi). \quad (32)$$

This will give a discrete set of solutions $\kappa_0 a = \xi_{n,m}$ for each n. For η and ε_z not very small, the values $\xi_{n,m}$ can be obtained approximately by making use of the asymptotic behavior $g_n(x) \sim x^{-1}$ for $x \to \infty$ and the Padé approximant of $f_n(x)$, which will be discussed in the Appendix. The anisotropic waveguide supports an infinite number of hybrid modes, no matter how thin the waveguide is.

Close to the light line, $\xi \to 0$, the eigenequation can be simplified. We consider the hybrid modes with different n separately.

For $n = 1$, one has $g_1(x) \simeq x^{-2} - \ln(x/2) - \gamma$ for $x \to 0$, thus Eq. (31) becomes

$$\varepsilon_z f_1(Ka) \simeq -2\left(\ln\frac{\xi}{2} + \gamma\right) + h_1(y) + \frac{1 + \varepsilon_t}{y^2} \quad (33)$$

with $\xi \ll y$. One has the solution $Ka \to x_{1,m}$ for $\xi \to 0$. Note that throughout this paper, we use $x_{n,m}$ to denote the mth zero of $J_n(x)$. Also that $x_{n,0} = 0$ for $n \geq 1$. Since $x_{1,0} = 0$, special care should be taken for solutions $Ka \sim 0$. Making use of the asymptotic behaviors $h_n(x) \simeq nx^{-2} + 1/[2(n+1)]$ and $f_n(x) \simeq nx^{-2} - 1/[2(n+1)]$ for $x \to 0$ with $n \geq 1$, one obtains

$$Ka \simeq \frac{1}{\eta} \sqrt{\frac{1 + \varepsilon_t}{\ln(\xi/2) + \gamma - (\varepsilon_z + 1)/8}}. \quad (34)$$

From this expression, one can see that only if $\varepsilon_t < -1$, there will be a solution for $Ka \sim 0$ when $\xi \to 0$. The above expression gives the dispersion of the first band with $n = 1$. The mth band will start with $Ka = x_{1,m-1}$ and end with $Ka = \xi_{1,m}/\eta$. One has $\xi_{1,1} < \eta x_{1,1}$. However if $-1 < \varepsilon_t < 0$, there will be no

solution for $Ka < x_{1,1}$. All the allowed modes will have finite Ka. For the mth band, one has $x_{1,m} \leq Ka \leq \xi_{1,m}/\eta$ with $\xi_{1,1} > \eta x_{1,1}$. The first band starts with $Ka = x_{1,1}$. For any $x_{1,m} > 0$, one has

$$Ka \simeq x_{1,m} - \frac{\varepsilon_t x_{1,m}}{(\eta x_{1,m})^2 \{-2[\ln(\xi/2) + \gamma] + h_1(\eta x_{1,m})\} + \varepsilon_t + 1}. \quad (35)$$

The hybrid modes near the light line with $n = 1$ are all forward waves.

For $n \geq 3$, one has the following asymptotic behavior of $g_n(x)$ for $x \to 0$,

$$g_n(x) \simeq \frac{n}{x^2} + \frac{1}{2(n-1)} + \alpha x^2, \quad (36)$$

with $\alpha = -1/[8(n-2)(n-1)^2]$. The eigenequation (31) is reduced to

$$\alpha^2 \xi^6 + c_2 \xi^4 + c_1 \xi^2 + c_0 = 0 \quad (37)$$

with

$$c_2 = \alpha\left(\frac{1}{n-1} + h_n - \varepsilon_z f_n\right),$$

$$c_1 = 2n\alpha + \frac{1}{4(n-1)^2} + \frac{h_n - \varepsilon_z f_n}{2(n-1)} - \varepsilon_z f_n h_n - n^2 \frac{\varepsilon_t}{y^4},$$

$$c_0 = \frac{n}{n-1} + n(h_n - \varepsilon_z f_n) + \frac{n^2(1 + \varepsilon_t)}{y^2}. \quad (38)$$

The eigenmodes on the light line are given by the equation $c_0 = 0$. The existence of solution requires that $c_0 \geq 0$. Only the positive root with small magnitude of the above cubic polynomial will give the dispersion for the modes near the light line. Since ξ is small, the physical solution can be approximated as $\xi^2 = -c_0/c_1 - c_2 c_0^2/c_1^3 - \alpha^2 c_0^3/c_1^4$. Those modes all have $Ka > x_{n,m}$ for the mth band.

For $n = 2$, the asymptotic behavior of $g_n(x)$ is still given by Eq. (36), but with a nonconstant coefficient $\alpha = [\ln(x/2) + \gamma]/4$. The eigenequation near the light line is reduced further from Eq. (37) to

$$(\kappa_0 a)^2\left(\ln\frac{\kappa_0 a}{2} + \gamma\right) + c_0 = 0 \quad (39)$$

with c_0 given in Eq. (38) with $n = 2$.

For the allowed eigenmodes of the mth hybrid band, one has the range $0 \leq \kappa_0 a < \xi_{n,m}$ with $\xi_{n,m}$ the solutions of Eq. (32). The solutions near both ends of the above range can be obtained analytically as we have done. For arbitrary ξ within this range, the solution must be obtained numerically. However only when $\varepsilon_t < -1$, one can have eigenmodes with $0 < Ka < x_{n,1}$. For the mth band, one has $x_{n,m} < Ka \leq \xi_{n,m}/\eta$. Otherwise, the solution for the first band requires $x_{n,1} < Ka \leq \xi_{n,1}/\eta$ with $\xi_{n,1} > \eta x_{n,1}$. The band structure for hybrid modes on a waveguide with $\varepsilon_t = -3$ and $\varepsilon_z = 2$ is shown in Fig. 8. The effective index of the waveguide $n_{\text{eff}} \equiv \beta/k_0$ is also evaluated and plotted in Fig. 9.
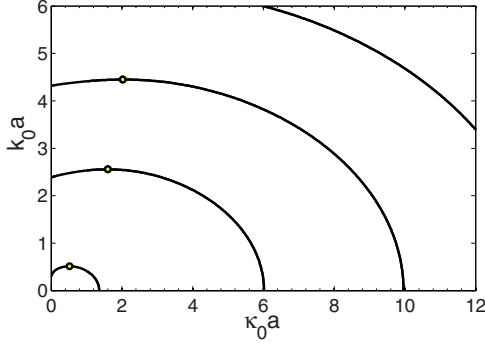
FIG. 8. (Color online) Band structure of the guided hybrid modes with $n=1$ on an anisotropic waveguide with $\varepsilon_t=-3$ and $\varepsilon_z=2$. Open circles denote the degeneracy of forward-wave and backward-wave modes.

2. Energy flow of hybrid modes

The energy flow can also be evaluated for hybrid modes. The expression for S_z is much more complex than that of the TM modes. However the final expression for P_z is much simpler than expected, once the integrals are all carried out. One has

$$P_z^{\text{in}} = \frac{\beta}{4k_0}\left[-\frac{\varepsilon_z^2}{\varepsilon_t Ka}(g_n+h_n)f_n' - \frac{1}{\kappa a}(g_n-\varepsilon_z f_n)h_n'\right.$$
$$\left. + \frac{2n^2}{(\kappa a)^4}\left(\frac{1+\varepsilon_t}{(\kappa_0 a)^2} - \frac{2\varepsilon_t}{(\kappa a)^2}\right)\right],$$

$$P_z^{\text{out}} = \frac{\beta}{4k_0}\left[-\frac{1}{\kappa_0 a}(2g_n+h_n-\varepsilon_z f_n)g_n'\right.$$
$$\left. - \frac{2n^2}{(\kappa_0 a)^4}\left(\frac{2}{(\kappa_0 a)^2} - \frac{1+\varepsilon_t}{(\kappa a)^2}\right)\right]. \quad (40)$$

Here f_n', g_n', and h_n' are the derivatives of f_n, g_n, and h_n, respectively. In this derivation, we assume ε_t and ε_z are real, thus the arguments of the Bessel functions are all real. We set
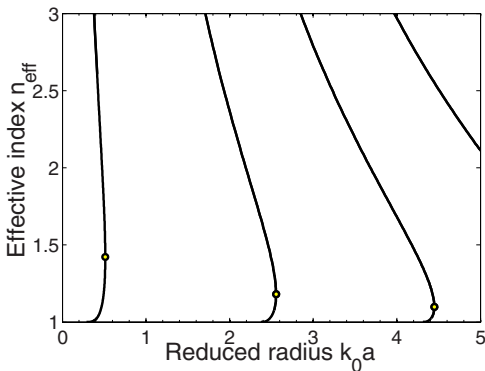

FIG. 9. (Color online) Effective index n_{eff} as a function of the reduced radius $k_0 a$ for the first three bands of hybrid modes with $n=1$ on an anisotropic waveguide with $\varepsilon_t=-3$ and $\varepsilon_z=2$. Open circles denote the degeneracy of forward-wave and backward-wave modes.

$A=\sqrt{g_n+h_n}/(k_0 a J_n)$. Use has also been made of the following integrals which cannot be found in any mathematics manual,

$$\int_0^x \left[J_n'^2(x) + \frac{n^2}{x^2}J_n^2(x)\right]x\,dx = -\frac{x^3}{2}J_n^2(x)f_n'(x),$$

$$\int_0^x \left[I_n'^2(x) + \frac{n^2}{x^2}I_n^2(x)\right]x\,dx = -\frac{x^3}{2}I_n^2(x)h_n'(x),$$

$$\int_x^\infty \left[K_n'^2(x) + \frac{n^2}{x^2}K_n^2(x)\right]x\,dx = -\frac{x^3}{2}K_n^2(x)g_n'(x). \quad (41)$$

Explicitly, one has

$$f_n'(x) = -xf_n^2(x) - \frac{2}{x}f_n(x) + \frac{n^2}{x^3} - \frac{1}{x},$$

$$h_n'(x) = -xh_n^2(x) - \frac{2}{x}h_n(x) + \frac{n^2}{x^3} + \frac{1}{x},$$

$$g_n'(x) = xg_n^2(x) - \frac{2}{x}g_n(x) - \frac{n^2}{x^3} - \frac{1}{x}. \quad (42)$$

We point out that the above expressions for P_z can be readily modified for dielectric or metallic cylindrical waveguide with the exchange of $f_n(ix)=-h_n(x)$ and $ixf_n'(ix)=-xh_n'(x)$.

The normalized energy flow on a waveguide with $\varepsilon_t=-3$ and $\varepsilon_z=2$ for the hybrid modes with $n=1,2,3$ is plotted in Fig. 10.

3. Backward-wave and forward-wave hybrid modes

The hybrid modes have similar features as the TM modes that both forward waves and backward waves can coexist within the same band. For $k_0 a \to 0$, $\kappa \simeq \kappa_0$, the hybrid modes have $d(k_0 a)/d(\kappa_0 a)<0$ and are all backward waves. Only the modes near the light line can be forward waves. Making use of the expressions for P_z in Eq. (40), one can prove that $d(k_0 a)/d(\kappa_0 a)\geq 0$ leads to $P_z \geq 0$ and vice versa. The degeneracy of forward- and backward-wave modes is located at $d(k_0 a)/d(\kappa_0 a)=0$ or $\langle P_z\rangle=0$.

For the hybrid modes with $n=1,2$, the modes near the light line are forward waves since $d(k_0 a)/d(\kappa_0 a)>0$. However, as can be seen in Fig. 10, the whole first band of the hybrid modes with $n=3$ are backward waves. Hybrid modes with higher n will have more bands to be all backward waves. If one further increases the angular index n of the hybrid modes, more hybrid mode bands will be all backward waves.

III. SLOW AND TRAPPED LIGHT

Recently Tsakmakidis *et al.* [31] proposed to trap light in a tapered waveguide with double negative index. The indefinite index waveguide we have studied so far in this paper can also be used to slow down and trap light. These waveguides can thus be used as optical buffers [32]. The reason is that unlike the ordinary optical fiber, these waveguides support both forward and backward waves.
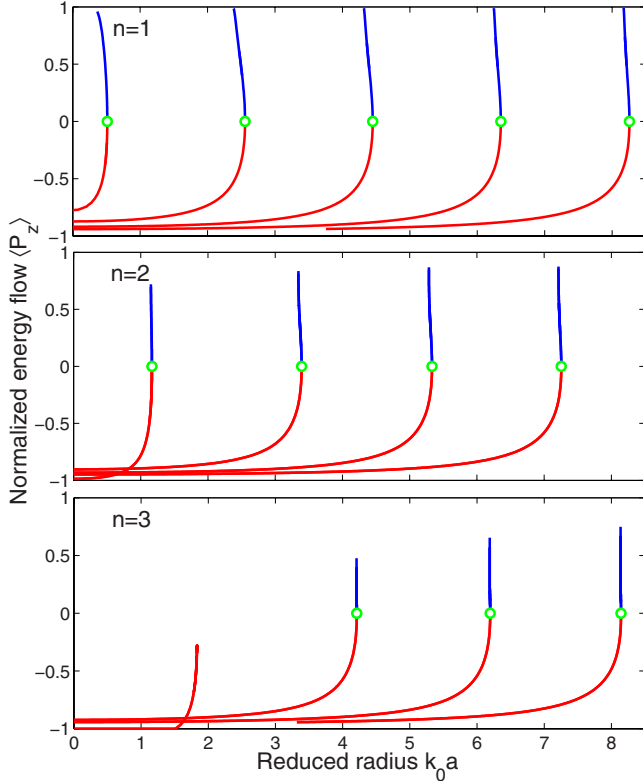
FIG. 10. (Color online) Normalized energy flow $\langle P_z \rangle$ for the first few bands of the hybrid modes with $n=1,2,3$ on an anisotropic waveguide with $\varepsilon_t = -3$ and $\varepsilon_z = 2$. Open circles denote the degeneracy points where $\langle P_z \rangle = 0$.

For the anisotropic waveguide we have considered, $\varepsilon_t < 0$, one has $P_z^{\text{in}} < 0$ and $P_z^{\text{out}} > 0$ if one sets $\beta > 0$. If $P_z = P_z^{\text{in}} + P_z^{\text{out}} < 0$, the mode is a backward mode since the total energy flow is opposite to the phase velocity. Otherwise, the mode is a forward mode. At the critical radius a_c, the backward and forward modes become degenerate; the energy flow inside the waveguide cancels out that in the air. One can prove that at the critical radius a_c where $P_z = 0$, the group velocity is indeed zero. One does not need to know the material dispersion to locate the zero group velocity point. This is due to the fact that for these waveguides, the dispersion due to geometric confinement dominates the material dispersion at and around the critical radius.

The unique properties of the modes on the anisotropic waveguide can be used to slow down and even trap light. Even though the waveguide supports infinite number of both TM and hybrid modes at any fixed radius and frequency, with appropriate laser coupling, the excitation of the hybrid modes in the waveguide can be suppressed or even eliminated. Among the TM modes, the first TM mode will be more favorably excited. Furthermore, due to the material dissipation, the first TM mode will propagate the longest distance. The rest of the TM modes will all decay out at about one-half the decay length of the first TM mode. It is the first TM band which can be used for slow light application. Unlike the double negative waveguide [31], the anisotropic waveguide will slow down and trap light if one increases the radius to the critical radius. A sketch of a slow light waveguide is shown in Fig. 11.
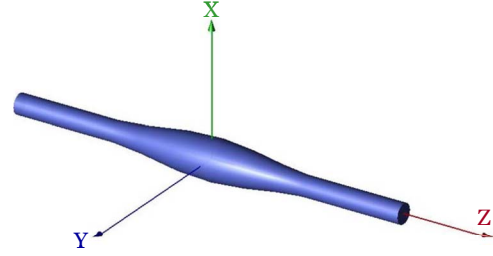

FIG. 11. (Color online) A sketch of the slow light waveguide.

IV. REALIZATION OF EXTREMELY ANISOTROPIC NANOWIRES

These extremely anisotropic media can be realized in metamaterials. According to the effective medium theory [33,26], one has for multilayered structure of dielectric ε_a and metal ε_m, the effective permittivity's

$$\varepsilon_t = f\varepsilon_m + (1-f)\varepsilon_a,$$

$$\varepsilon_z = \frac{\varepsilon_a \varepsilon_m}{f\varepsilon_a + (1-f)\varepsilon_m}. \tag{43}$$

Here f is the filling ratio of the metal. For $f > f_{\min} \equiv \varepsilon_a / (\varepsilon_a - \text{Re }\varepsilon_m)$, one has $\text{Re }\varepsilon_t < 0$. A realization of the anisotropic nanowire is shown in Fig. 12.

We first consider a metamaterial waveguide at a fixed wavelength. For silver at $\lambda = 488$ nm, one has $\varepsilon_m = -9.121 + 0.304i$ [34]. A nanowire made of alternative disks of silver and glass ($\varepsilon_a = 2.25$) of equal thickness will have $\varepsilon_t = -3.436 + 0.152i$ and $\varepsilon_z = 5.971 + 0.065i$ by using the effective medium theory. Here the disk thickness is 10 nm for both materials. For example, if one sets $a = 60$ nm, one has $k_0 a = 0.7725$. The first three TM modes will have $\beta a = 2.2525 - 0.0747i, 4.9318 - 0.1419i, 7.4031 - 0.2088i$. Thus one has $\lambda_\beta \sim 167$ nm and phase refractive index $n_{\text{eff}} = 2.92$ for the first TM mode. The decay length is 803, 423, and 287 nm, respectively. After traveling about 420 nm along the nanowire, only the first one will survive.

Finite-difference time-domain (FDTD) simulations [35] were performed to obtain the effective index n_{eff} of the metamaterial nanowire. The procedure is the following. We illuminate the free-standing nanowire of finite length with a Gaussian beam, then get E_z after the termination of the simulation. The length of the waveguide is set to be larger than the decay length of the first TM mode. We get the phase from
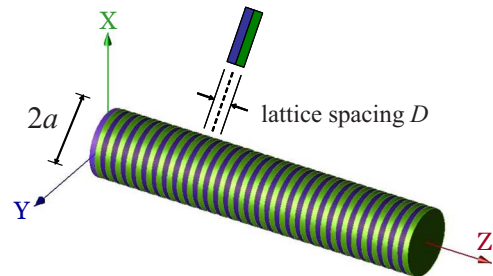

FIG. 12. (Color online) A sketch of the realization of an anisotropic nanowire made of alternative disks of metal and dielectric.
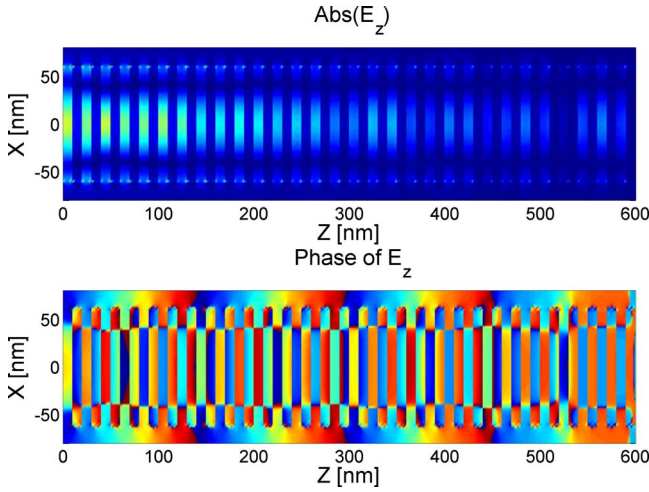
FIG. 13. (Color online) FDTD simulation of the amplitude and phase propagation of the longitudinal electric field E_z along the nanowire with radius $a=60$ nm at $\lambda=488$ nm. The metamaterial nanowire consists of alternative disks of silver and glass disks of thickness 10 nm.

E_z, then determine β. Though the waveguide supports infinite number of modes including TM and hybrid modes, our method is legitimate due to the following two reasons. First that the excitation of hybrid modes is small due to the profile of the incident Gaussian beam. So mainly the TM modes are excited. Second that due to the dissipation in the metal, after certain distance, only the first TM mode will survive. Thus, the phase propagation is mainly due to the first TM mode. The amplitude and phase propagation of E_z along the above metamaterial nanowire is shown in Fig. 13.

The relation between the effective index n_{eff} and the nanowire radius a is shown in Fig. 14. Very good agreement between FDTD simulations and analytical results has been obtained. However, for small radius, there is noticeable discrepancy. This is expected since when the radius is comparable with the lattice spacing of the multilayered metamate-
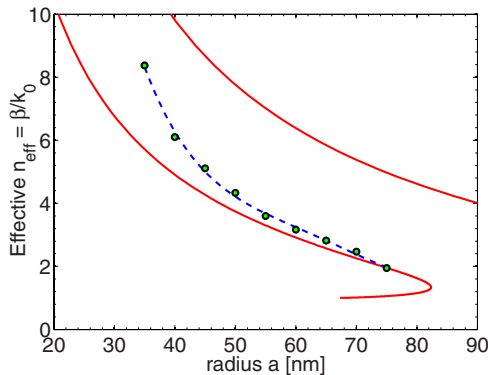

FIG. 14. (Color online) The effective index n_{eff} of the first TM band on a nanowire with different radius at $\lambda=488$ nm. The nanowire is made of alternative disks of silver and glass (see Fig. 12). The disk thickness is 10 nm. Filled circle (green) is obtained from FDTD simulations. The dashed line (blue) is the fitting of simulation data. The solid line (red) is calculated from band equation with effective index $\varepsilon_t=-3.436+0.152i$ and $\varepsilon_z=5.971+0.065i$.
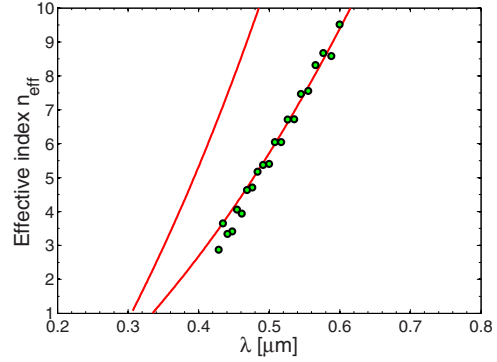

FIG. 15. (Color online) The effective index n_{eff} for the TM modes on a nanowire with radius $a=40$ nm. The nanowire is a stack of equally thick alternative disks made of a Drude metal $\varepsilon_m=1-k_p^2/k_0(k_0+i\Gamma)$ and glass. Here $k_p a=1.64$ and $\Gamma a=0.0155$. The analytical curves (solid) are calculated by using real ε_m.

rial, the effective medium theory will fail. We have also performed FDTD simulations for the nanowire with smaller lattice spacing. Better agreement is indeed obtained.

We also consider the band structure for different frequencies. The permittivity given by Eq. (24) can be realized through the multilayered heterostructure with Drude metal with $\varepsilon_m=1-k_p^2/k_0$ and dielectric ε_a. The nanowire is made of alternative disks of a Drude metal and a dielectric. The band structure and the effective index n_{eff} of the TM modes are shown in Fig. 4 and Fig. 5, respectively. One noticeable feature of these bands is the flatness of each band, which indicates small group velocity. We have performed the FDTD simulation for different frequencies for a nanowire with a fixed radius. The results are shown in Fig. 15. Again good agreement between FDTD simulations and analytical results is achieved.

V. CONCLUSIONS

Indefinite index materials can be used to achieve negative refraction [25] and hyperlensing [27,28]. They can also be used as superlens [26]. In this paper, we consider the wave propagation along a cylindrical waveguide with anisotropic optical constant. We have derived the eigenmodes equation and obtained the solutions for all the propagation modes. The field profiles and the energy flow on the waveguide are also analyzed. Closed-form expressions for the energy flow for all the modes are derived. For extremely anisotropic cylinder where the transverse component of the permittivity is negative and the longitudinal is positive ($\varepsilon_t<0$, $\varepsilon_z>0$), the waveguide supports TM and hybrid modes but not the TE modes. Among the supported TM modes, at most only one mode can be a forward wave. The rest of them are backward waves.

The case that $\varepsilon_t>0$ and $\varepsilon_z<0$ can be discussed similarly. Anisotropic waveguides of cross section other than a circle were also considered. The results will be presented elsewhere.

Possible realizations of these extremely anisotropic nanowires are proposed. Extensive FDTD simulations have been

performed and confirmed our analytical results.

Two unique properties have been revealed for the modes on nanowire waveguides made of indefinite index metamaterials. The first is that the backward-wave modes can have very large effective index. These nanowires can be used as phase shifters and filters in optics and telecommunication. The second is that the waveguide supports modes of zero group velocity. This is due to the fact that the waveguide can support both forward and backward waves at a fixed radius. If the waveguide is tapered, at certain critical radius, the two modes will be degenerate and carry zero net energy flow. At other radii, these waveguides support modes with small group velocity. These waveguides can also be used as an ultracompact optical buffer [32] in integrated optical circuits.

APPENDIX: PADÉ APPROXIMANT OF $f_n(x)$

Consider the function $f_n(x) = J'_n(x)/[x J_n(x)]$. Let $x_{n,m}$ be the mth zero of the Bessel function $J_n(x)$. We also denote $x'_{n,m}$ as the zeros of $J'_n(x)$. In order to get the eigenmodes on the anisotropic waveguide easily, we may need the inverse function $f_n^{-1}(x)$ in the interval $[x_{n,m}, x'_{n,m}]$. We consider the Padé approximant to the function $f_n(x)$,

$$f_n(x) \simeq \frac{(x - x'_{n,m})(x - x_{n,m} - b)}{c(x - x_{n,m})(x - x_{n,m} - a)}. \tag{A1}$$

Instead of fixing the three unknowns through the coefficients of the Taylor expansion of $f_n(x)$, here we determine them by the exact values of $f_n(x)$ at some points. Since there are three unknowns, we only need the value of $f_n(x)$ at three points. For simplicity, we evaluate $f_n(x)$ at three evenly spaced points,

$$f_{n,j} \equiv f_n(x_{n,m} + j\Delta/4) \tag{A2}$$

for $j = 1, 2, 3$. Here $\Delta = x'_{n,m} - x_{n,m}$. One thus has $f_{n,j} = (4 - j)(j\Delta - 4b)/[jc(j\Delta - 4a)]$. We further define

$$\sigma_1 = 3f_{n,2}/f_{n,1}, \quad \sigma_2 = 3f_{n,3}/f_{n,2}. \tag{A3}$$

After some manipulations of the algebra, one obtains

$$a = \frac{\Delta}{4}\left(2 + \frac{\sigma_2 - \sigma_1^{-1}}{\sigma_2 + \sigma_1^{-1} - 2}\right),$$

$$b = \frac{\Delta}{4}\left(2 - \frac{\sigma_1 - \sigma_2^{-1}}{\sigma_1 + \sigma_2^{-1} - 2}\right),$$

$$c = -\frac{1}{f_{n,2}}\frac{\Delta - 2b}{\Delta - 2a}. \tag{A4}$$

The inverse of the function $f_n(x)$ can be obtained as one of the roots of a quadratic equation. As it turns out, the expression obtained in this way gives very good approximation to $f_n^{-1}(x)$.

Once the inverse function is obtained, one has $Ka = f_0^{-1}(y)$ with $y = g_0(\kappa_0 a)/\varepsilon_z$ for the TM modes. Together with the asymptotic expressions of $g_n(x)$ and $h_n(x)$, Eq. (A1) can also be used to obtain approximate solutions of the hybrid modes.

[1] V. Veselago, Sov. Phys. Usp. **10**, 509 (1968).

[2] R. A. Shelby, D. R. Smith, and S. Schultz, Science **292**, 77 (2001).

[3] J. B. Pendry, Phys. Rev. Lett. **85**, 3966 (2000).

[4] W. T. Lu and S. Sridhar, Opt. Express **13**, 10673 (2005).

[5] W. T. Lu and S. Sridhar, Microw. Opt. Technol. Lett. **39**, 282 (2003).

[6] N. Fang *et al.*, Science **308**, 534 (2005).

[7] P. Vodo, P. V. Parimi, W. T. Lu, and S. Sridhar, Appl. Phys. Lett. **86**, 201108 (2005).

[8] P. Vodo, W. T. Lu, Y. Huang, and S. Sridhar, Appl. Phys. Lett. **89**, 084104 (2006).

[9] C. G. Parazzoli, R. B. Greegor, K. Li, B. E. C. Koltenbah, and M. Tanielian, Phys. Rev. Lett. **90**, 107401 (2003).

[10] P. V. Parimi, W. T. Lu, P. Vodo, J. Sokoloff, J. S. Derov, and S. Sridhar, Phys. Rev. Lett. **92**, 127401 (2004).

[11] P. V. Parimi, W. T. Lu, P. Vodo, and S. Sridhar, Nature (London) **426**, 404 (2003).

[12] E. Cubukcu *et al.*, Nature (London) **423**, 604 (2003).

[13] Z. Lu, J. Murakowski, C. Schuetz, S. Shi, G. Schneider, and D. Prather, Phys. Rev. Lett. **95**, 153901 (2005).

[14] A. Berrier, M. Mulot, M. Swillo, M. Qiu, L. Thylen, A. Talneau, and S. Anand, Phys. Rev. Lett. **93**, 073902 (2004).

[15] G. Dolling, C. Enrich, M. Wegener, C. M. Soukoulis, and S. Linden, Science **312**, 892 (2006).

[16] C. M. Soukoulis, S. Linden, and M. Wegener, Science **315**, 47 (2007).

[17] D. R. Smith, J. B. Pendry, and M. C. Wiltshire, Science **305**, 788 (2004).

[18] M. Notomi, Phys. Rev. B **62**, 10696 (2000).

[19] B. Gralak, S. Enoch, and G. Tayeb, J. Opt. Soc. Am. A **17**, 1012 (2000).

[20] C. Luo, D. G. Johnson, J. D. Joannopoulos, and J. B. Pendry, Phys. Rev. B **65**, 201104(R) (2002).

[21] V. M. Shalaev, Nat. Photonics **1**, 41 (2007).

[22] J. D. Joannopoulos, R. D. Meade, and J. N. Winn, *Photonic Crystals: Molding the Flow of Light* (Princeton University Press, Princeton, NJ, 1995).

[23] D. Schurig, J. J. Mock, B. J. Justice, S. A. Cummer, J. B. Pendry, A. F. Starr, and D. R. Smith, Science **314**, 977 (2006).

[24] D. R. Smith and D. Schurig, Phys. Rev. Lett. **90**, 077405 (2003); D. R. Smith, P. Kolinko, and D. Schurig, J. Opt. Soc. Am. B **21**, 1032 (2004).

[25] A. J. Hoffman *et al.*, Nat. Mater. **6**, 946 (2007).

[26] W. T. Lu and S. Sridhar, Phys. Rev. B **77**, 233101 (2008).

[27] Z. Liu *et al.*, Science **315**, 1686 (2007).

[28] I. I. Smolyaninov, Y.-J. Hung, and C. C. Davis, Science **315**, 1699 (2007).

[29] J. Takahara *et al.*, Opt. Lett. **22**, 475 (1997).

[30] K. L. Tsakmakidis, A. Klaedtke, D. A. Aryal, C. Jamois, and O. Hess, Appl. Phys. Lett. **89**, 201103 (2006).

[31] K. L. Tsakmakidis, A. D. Boardman, and O. Hess, Nature (London) **450**, 397 (2007).

[32] F. Xia, L. Sekaric, and Y. Vlasov, Nat. Photonics **1**, 65 (2007).

[33] A. Sihvola, *Electromagnetic Mixing Formulas and Applications* (Institute of Electrical Engineers, London, 1999).

[34] E. D. Palik, *Handbook of Optical Constants of Solids* (Academic, New York, 1981).

[35] A. Taflove and S. C. Hagness, *Computational Electrodynamics: The Finite-Difference Time-Domain Method*, 3rd ed. (Artech House, Norwood, MA, 2005).